Dalton Transactions

ARTICLE

Coupling molecular spin centers to microwave planar resonators: towards integration of molecular qubits in quantum circuits

Received 00th January 20xx,
Accepted 00th January 20xx

DOI: 10.1039/x0xx00000x

www.rsc.org/

C. Bonizzoni,[a,b] A. Ghirri,[b] K. Bader,[c] J. van Slageren,[c] M. Perfetti,[d] L. Sorace,[d] Y. Lan,[e] O. Fuhr,[e] M. Ruben[e,f] and M. Affronte[a,b]

We present spectroscopic measurements looking for the coherent coupling between molecular magnetic centers and microwave photons. The aim is to find the optimal conditions and the best molecular features to achieve the quantum strong coupling regime, for which coherent dynamics of hybrid photons-spin states take place. To this end, we used a high critical temperature YBCO superconducting planar resonator working at 7.7 GHz and at low temperatures to investigate three molecular mononuclear coordination compounds, namely Cu(mnt)$_2$, [ErPc$_2$]$^-$ TBA$^+$ and Dy-trensal. Although the strong coupling regime was not achieved in these preliminary experiments, results provide several hints on how to design molecular magnetic centers to be integrated into hybrid quantum circuits.

Introduction

In the last years we have been exploring the possibility to coherently manipulate molecular magnetic moments (hereafter also referred as "molecular spins" for simplicity). The challenge we wish to tackle is to move a step ahead with respect to the control of static magnetic characteristics of molecules and to exploit their genuine quantum features, such as the superposition of molecular states or their quantum correlation (also referred to as "entanglement") [GTA]. However, coherent superposition states are fragile since the environment induces decoherence [DEC]. Key experiments are usually performed by pulsed Electron Spin Resonance which allow characterization of both spin-lattice relaxation as well as dephasing while observation of Rabi oscillations are used as to test if coherence life time of the molecular spin is sufficiently long to be preserved by decoherence mechanisms.

We have recently adapted a circuit on a chip, normally used for circuit-Quantum Electro Dynamics (QED) experiments [Nori], to manipulate molecular spins by microwave photons in a planar resonator [APL]. The use of superconductors allows fabrication of planar cavities with high quality factor (Q) and resonance frequencies (ω_0) typically in the 2-10 GHz range, thus performing Electron Paramagnetic Resonance (EPR) spectroscopy with very high sensitivity [Bienfait]. However, by using a low number of photons (significantly lower than the number of spins in the sample) it is possible to achieve a working regime for which coherent coupling between cavity photons and a spin ensemble is obtained. This is the case in which the collective system can be described by the Tavis-Cummings Hamiltonian, leading to hybridized spin-photon modes and Rabi oscillations [TavisCummings]. Such coherent dynamics, however, is achieved only when the coupling strength (Ω) between photons and spins exceeds the damping rates of both resonant cavity ($\kappa_0 = \omega_0/Q$) and spin system (γ). This is generally expressed by the so-called *strong coupling condition*, $\Omega >> \kappa_0, \gamma$. While this condition is relatively ease to achieve with electric dipoles, the coupling to magnetic centers is, in general, much weaker and decoherence mechanisms - still- hard to control [Nori, GTA]. However, some recent experiments have demonstrated that such *strong coupling regime* can be obtained at very low temperatures (<<1 K) with electronic spin ensemble provided by Nitrogen Vacancy (NV) centers in diamond or other spin impurities in crystals [spin_impurities], in particular in the erbium(III) doped crystalline inorganic compound matrix Er(III):YSi_2O_5 [Er_doped]. Inspired by these results, we have recently demonstrated that high T_c superconducting resonators can be used to achieve the strong coupling with organic radicals [APL,PyBTM] at finite temperature(T>1K). Notice that there is a clear signature of this *strong coupling regime* due to the appearance of two distinct branches in the frequency spectrum measured when the spin system is driven in

[a] Dipartimento FIM, Università di Modena e Reggio Emilia, via Campi 213/a, 411125 Modena, Italy.
[b] Istituto Nanoscienze - CNR, via Campi 213/a, 411125 Modena, Italy.
[c] Institut für Physikalische Chemie, Universität Stuttgart, Pfaffenwaldring 57, 70569 Stuttgart, Germany.
[d] Dipartimento di Chimica "U. Schiff" and UdR INSTM, Università di Firenze, Via della Lastruccia 3-13, Sesto Fiorentino(FI), Italy.
[e] Institute of Nanotechnology, Karlsruhe Institute of Technology (KIT), D-76344 Eggenstein-Leopoldshafen, Germany.
[f] Institut de Physique et Chimie des Matériaux de Strasbourg, UMR 7504 UdS-CNRS, 67034 Strasbourg Cedex 2, France.

Electronic Supplementary Information (ESI) available: [details of any supplementary information available should be included here]. See DOI: 10.1039/x0xx00000x

resonance with the cavity frequency [Abe]. This feature allows to distinguish from a conventional EPR spectroscopy, in which experiments are done in the weak coupling regime.

In this context, we investigated whether other magnetic molecules can be suitable for this type of coherent spin manipulation. The recipe looks simple: *a)* strong coupling with the magnetic component of electromagnetic wave and *b)* low decoherence, i.e. sharp resonance linewidth. With these guidelines in mind, we have started to search optimal molecular systems for the above-mentioned circuit-QED experiments. We have focused our attention on mononuclear complexes, since molecules with simple structures and nuclear spin free ligands –in principle- suffer less from decoherence. Good candidates must have sufficiently long coherence times and recently good examples of these have been presented in literature [long_Tm]. For instance, mononuclear $[Cu(mnt)_2]^{2-}$ molecules were found to be very promising, showing extraordinary long relaxation times at low-temperatures and quantum coherence even at room temperature [bader]. At the same time, we wish to enhance the magnetic coupling with photons and for this we need to look for molecules with favourable magnetic resonance transition matrix elements. In this respect, lanthanides based derivatives look very promising because of their high magnetic anisotropy. Moreover, the possibility to engineer the ligand field through the coordination geometry, make this class of molecules very attractive.

In this work we present preliminary circuit-QED experiments to test the magnetic coupling between selected molecular spin ensembles and a superconducting YBCO coplanar resonator. A mononuclear copper compound, $(PPh_4)_2[Cu(mnt)_2]$ (mnt=maleonitriledithiolate or 1,2-dicyanoethylene-1,2-dithiolate) and two Rare-Earth-based monometallic SMMs, $[ErPc_2]^-TBA^+$ (TBA^+=tetra-*n*-butylammonium cation) and Dy-trensal (H_3trensal=Tris[2-(salicylideneamino)ethyl]amine) with different concentrations and dilutions in diamagnetic analogues are studied. Results are compared also with similar experiments performed with spin impurities in inorganic matrices and organic radicals.

Experimental

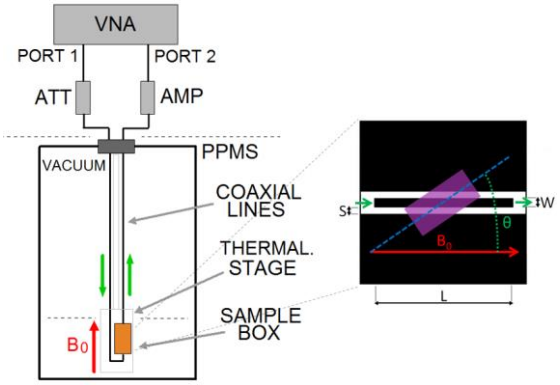

Figure 1. Left. Schematic diagram of the experimental set-up. Right. Top view of the YBCO coplanar resonator (black) with a crystal loaded on top (purple). The red arrow indicates the applied magnetic field, while the green ones the propagation of the TEM microwave signal. θ is the angle between the static magnetic field and the crystal c-axis.

a. Experimental set-up

Transmission spectroscopy experiments were carried out by means of a high critical temperature YBCO/sapphire coplanar resonator, which is installed in a commercial cryo-magnetic set-up (Quantum Design PPMS-7T) for measurements in varying temperatures and applied magnetic fields (Figure 1). The transmission scattering parameter (T) was measured as function of frequency (ν) by means of a vector network analyzer (Agilent PNA 26GHz). Measurements at low microwave powers (down to -70 dBm), were carried out with two attenuators and two amplifiers installed at room temperature. The resonator is located in a high-conductivity copper box, where two floating pins inject microwaves in the coplanar resonator. The extension of the pins can be regulated to adjust the coupling with the external input and output lines. The resonator is placed in correspondence of the centre of the superconducting coil and the magnetic field is applied parallel to the central YBCO strip. Our resonators are fabricated by optical lithography of YBCO/sapphire films, as reported in [APL]. The transmission spectrum of the bare resonator shows that $\omega_0/2\pi = 7.764$ GHz and $Q \approx 33000$ at 2 K (ESI). These parameters are remarkably stable in applied magnetic field [APL].

b. Molecular magnetic complexes

$Cu(mnt)_2$

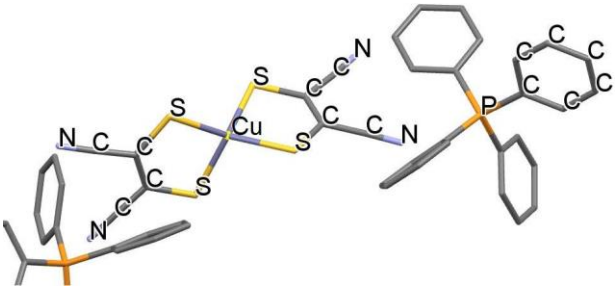

Figure 2: Crystal structure of the $(PPh_4)_2[Cu(mnt)_2]$ molecule. H atoms are omitted for clarity and the second PPh_4^+ ion is only partially shown.

The coordination compound $(PPh_4\text{-}d_{20})_2[Cu(mnt)_2]$ (where mnt^{2-} = maleonitriledithiolate or 1,2-dicyanoethylene-1,2-dithiolate), hereafter $Cu(mnt)_2$ in short, is shown in Figure 2. The Cu^{II} ion is coordinated to the sulfur atoms of the two dithiolate ligands, while two PPh_4^+ groups balance the dinegative charge of metal ion. $Cu(mnt)_2$ crystallizes in a monoclinic space group with two molecules related by a 2_1 screw axis, leading to two different orientations in the unit cell. [Lewis].

The powder EPR spectrum of $Cu(mnt)_2$ [Bader] shows eight resonance lines resulting from an axial *g*-tensor and an anisotropic hyperfine interaction between the electron (S = 1/2) and nuclear spin (I = 3/2) of the Cu(II)-ion. The *g*-factors obtained from the spectral fit provided $g_{||}$ =2.0925 and $g_{\perp}$ = 2.0227 [Bader].

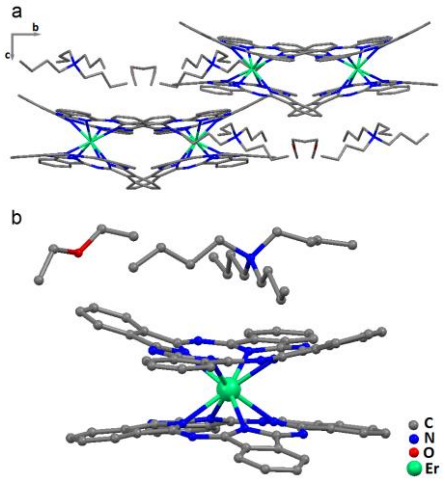

Figure 3: Molecular structure of $[ErPc_2]^-[TBA]^+$. Hydrogen atoms were omitted for clarity. (a) Packing diagram of $[ErPc_2]^-[TBA]^+$, showing the positions of the $[TBA]^+$ cations and diethylether solvent molecules in the unit cell. (b) The molecular structure of $ErPc_2^-[TBA]^+$ showing the Er(III) metal ion (green) coordinated by the isoindole nitrogens (blue). The thermal ellipsoids in $[ErPc_2]^-$ were drawn at 50% of probability.

$ErPc_2$ double-decker

Single crystals suitable for X-ray diffraction analysis were obtained by slow diffusion of Et_2O into a solution of $[ErPc_2]^-[TBA]^+$ complex in acetonitrile as fine dark purple needles. This anionic form consists of a trivalent lanthanide ion (Er^{+3}) coordinated by two Pc ligands, each one bearing a formal charge of –2. The organic core adopts a closed shell π-electronic configuration. The resulting negative charge located on $[ErPc_2]^-$ is stabilized by a counter cation, such as bulky *n*-tetrabutylammonium $[TBA]^+$. A view of the molecular structure of $[ErPc_2]^-[TBA]^+$ is depicted in Figure 3(b). The $[ErPc_2]^-[TBA]^+$ complex crystallizes in the orthorhombic space group $Pna2_1$ with four molecules per unit cell which belong to two tilted sub-lattices: a subset of molecules has Pc planes rotated by 10° with respect to the ab plane of the crystal, while the other subset has Pc planes rotated by 160° with respect to the first one (see Figure 3(a)). This structure was not previously reported in literature and further details are given in the ESI.

The magnetic properties of the $ErPc_2$ double-decker are characterized by an easy-plane anisotropy, which lifts the degeneracy of the $J = 15/2$ total angular momentum of the Er^{III} ion, giving a Kramers $M_J = \pm 1/2$ ground doublet well separated from the first excited state ($M_J = \pm 3/2$), which becomes significantly populated above 30 K [Ishikawa03, Marx]. The easy plane anisotropy gives rise to a large effective perpendicular g-factor $g_\perp = 9.59$ in the plane of the phthalocyanines, similar to what reported in [Marx]. Erbium has one isotope with non-zero nuclear spin ^{167}Er ($I = 7/2$, abundance of 23%).

Dy-trensal

Dy-trensal is a single ion magnet based on Dy(III) bound by the triply depronotated form of the H_3trensal = 2,2',2"-Tris-(salicylideneimino)triethylamine) ligand (Figure 4). The system crystallizes in the trigonal P$\bar{3}$c1 space group, the Dy(III) and the tertiary aminic nitrogen of the ligand sitting on the crystallographic C_3 axis. The molecular symmetry is thus exactly trigonal, with the principal anisotropy axis coincident with the crystallographic *c* axis of the unit cell as also demonstrated by the low temperature luminescence spectra [Flanagan]. Hexagonal, needle-shaped single crystals of Dy-trensal, synthesised as previously reported for the isostructural Er(III) analogue [Pedersen], typically grow with the crystallographic *c* axis as the longest dimension of the crystal [Perfetti]. The unit cell contains four molecules packed with an enantiomeric displacement: however, since the Dy(III) ions lies in a special position, the principal axes of all the molecules are iso-oriented. The crystal field parameters of Dy-trensal, previously obtained by luminescence spectra [Flanagan] and Cantilever Torque Magnetometry [Perfetti] revealed the easy plane nature of the magnetic anisotropy of Dy(III) in this molecule. This was further corroborated by the analysis of EPR spectra [Lucaccini], providing an anisotropic effective *g*-tensor with $g_{||} = 1.8$ along the (hard) *z*-axis and $g_\perp = 9.4$ in the perpendicular (easy) plane. Dy has 7 stable isotopes (^{156}Dy, ^{158}Dy, ^{160}Dy, ^{161}Dy, ^{162}Dy, ^{163}Dy, ^{164}Dy). Their nuclear spin is $I = 0$ for the even isotopes, and $I = 5/2$, for the odd ones.

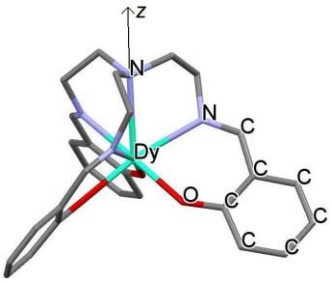

Figure 4: X-ray structure of the Dy-trensal molecule. Colour scheme: Dy, cyan; O, red; N, violet; C, grey. H atoms are omitted for clarity.

Results and discussion

a. Transmission Spectroscopy Experiments

For each compound we have investigated crystals with different concentrations of magnetic centers and at different orientations with the respect to the applied magnetic field. Hereafter we report the main results referring the reader to ESI for more complete data sets.

We initially investigated **$Cu(mnt)_2$** single crystals. On a non-diluted $Cu(mnt)_2$ crystal we observed four broad resonances centered at ≈ 0.27 T which corresponds to a Landé *g*-factor of 2.04 (Figure S2 of the ESI). Better resolved structures in the spectrum (Figure 5) were obtained on a crystal of $Cu(mnt)_2$ doped into the diamagnetic analogue $(PPh_4\text{-}d20)_2[Ni(mnt)_2]$ (concentration of ca. 2%). The shift of the cavity frequency and the variation of the linewidth are plotted in Figure 5 as a function of the magnetic field. Lowering the temperature from

20 to 2 K results in a progressive increase of the intensity of the transitions and in their narrowing. The four principal structures can be ascribed to the hyperfine splitting in $Cu(mnt)_2$, which is due to the presence of the nuclear magnetic moment of Cu(II), while the finer structure is due to the fact that two orientations of the molecules are present in the crystal. The angular dependence of the measured spectra, reported in Figure S3 of the ESI, is consistent with EasySpin simulations carried out with an anisotropic hyperfine Hamiltonian, as discussed in Ref.[Bader] and ESI.

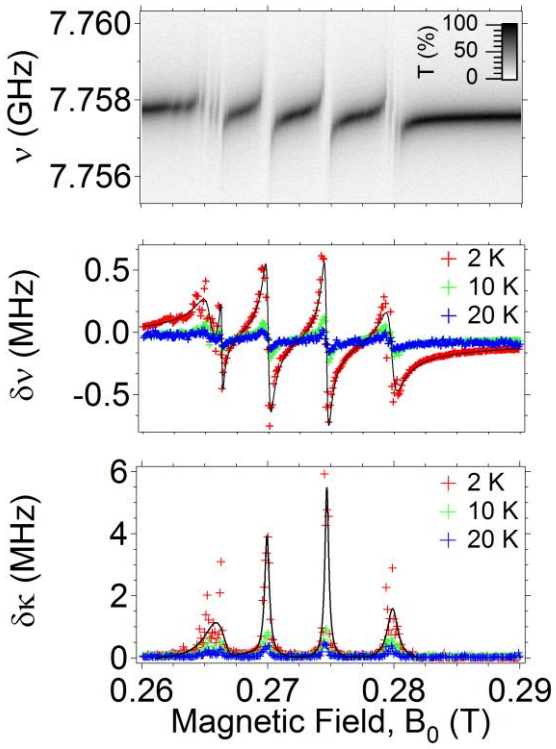

Figure 5: (Upper panel) Transmission spectral map measured at 2 K for a diluted (2%) and deuterated single crystal of $Cu(mnt)_2$ (P_{in} = -63 dBm, θ=90°). (Middle panel) Field dependence of the shift of the resonator frequency and (lower panel) the relative variation of the linewidth. Data taken at 2, 10 and 20 K are shown for comparison. Solid lines display the fitting curve with Eq. 1a and 1b.

We investigated single crystals of **$[ErPc_2]^-TBA^+$** molecules dispersed in the diamagnetic analogue $[YPc_2]^-TBA^+$ with different concentrations. Needle-shaped crystals were aligned with the crystallographic *c*-axis either parallel (θ=0°) or perpendicular (θ=90°) to the static magnetic field. Figure 6 shows the experimental data obtained on a $[ErPc_2]^-TBA^+$ 10% diluted crystal oriented at θ=90°. For this orientation the two sets of molecules have the same symmetric displacement (10°) of the Pc planes with respect to the external magnetic field. The transmission spectral map shows a resonance at ≈0.061 T (upper panel of Figure 6), which is accompanied by a shift of the cavity frequency and to an increase of the linewidth (middle and lower panel, respectively). For this resonance, the extracted *g*-factor is ≈ 9.2, which is consistent with the value reported in Ref. [Marx]. The transmission spectra measured for θ=0° show the shift of the main resonance toward lower *g*-factors, as it is expected from the easy plane anisotropy of the $[ErPc_2]^-TBA^+$ molecule (Figure S4 of the ESI). Other weaker transitions, which are observed in the range between 0.04 and 0.08 T, can be ascribed to the hyperfine components of the magnetic resonance line.

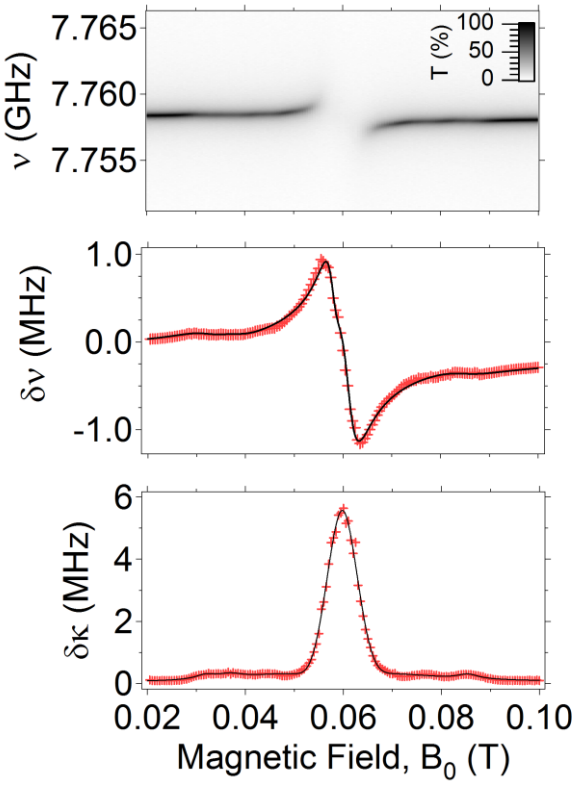

Figure 6: (Upper panel) Transmission spectral map measured at 2 K for a diluted (10%) $[ErPc_2]$-TBA+ single crystal (P_{in} = -43 dBm, θ=90°). (Middle panel) Field dependence of the shift of the resonator frequency and (lower panel) variation of the linewidth. Solid lines display the fitting curve with Eq. 1a and 1b.

We investigated single-crystals of **Dy-trensal** dispersed (3%) in isomorphous and diamagnetic Y-trensal. A needle-shaped single crystal was positioned at the centre of the resonator and aligned with the crystallographic *c*-axis perpendicular to the applied magnetic field (θ=90°). The experimental results are shown in Figure 7. An intense resonance is measured at ≈0.059 T, which corresponds to $g_\perp \approx 9.4$. Weak additional resonances, which are located symmetrically with respect to the central one, can be attributed to the hyperfine splitting in $I \neq 0$ Dy isotopes. Measurements taken at θ=0° show the shift of the main resonance to lower *g*-factors, as expected from the easy-plane effective anisotropy of Dy-trensal (Figure S6 of the ESI).

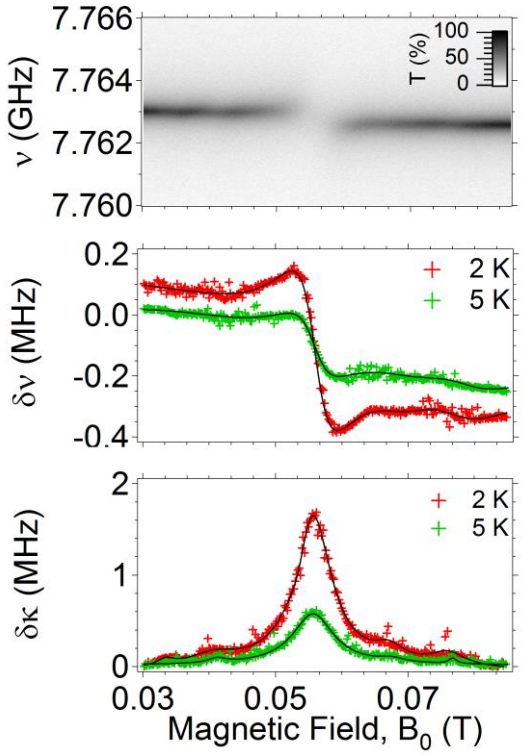

Figure 7: (Upper panel) Transmission spectral map measured at 2 K for a diluted (3%) single crystal of Dy-trensal (P_{in} = -43 dBm, θ=90°). (Middle panel) Field dependence of the shift of the resonator frequency and (lower panel) variation of the linewidth. Data taken at 2 and 5 K are shown for comparison. Solid lines display the fitted curve with Eq. 1a and 1b.

b. Discussion

Modelling the QED circuit. Within the framework of a lumped elements model, the microwave cavity behaves as a RLC resonator and the coupling with the spin ensemble is introduced through the dynamic susceptibility $\chi = \chi' - i\chi''$, where χ' and χ'' are respectively the field-dependent real (dispersive) and imaginary (absorptive) parts [Abragam, Bushev]. The susceptibility of the sample affects the inductance $L_0' = L_0(1 + \chi'\xi)$ and the resistance $R_0' = R_0 + \nu_0 L_0 \xi \chi''$, where L_0 and R_0 are the inductance and the resistance of the bare resonator respectively and ξ is the filling factor, which takes into account the fraction of the resonator volume filled by the spins. We assume that the bare capacitance (C_0) is unperturbed by χ. The resonant frequency and the quality factor of the resonator become $\nu_0' = 1/\sqrt{L_0' C_0} = \nu_0/\sqrt{1 + \chi' \xi}$ and $Q_0' = \nu_0' R_0' C_0$ resulting in a linewidth of the resonant peak of $\kappa_0' = \frac{\nu_0'}{Q_0'}$. Assuming weak coupling ($\chi'\xi \ll 1$) and no saturation, we have:

$$\nu_0' = \nu_0 + \frac{\Omega^2(\nu_0 - g\mathrm{x})}{(\nu_0 - g\mathrm{x})^2 + \gamma^2} \qquad (1a)$$

$$\kappa_0' = \kappa_0 + \frac{\Omega^2 \gamma}{(\nu_0 - g\mathrm{x})^2 + \gamma^2} \qquad (1b)$$

which describe the dispersive shift of the resonant peak and its broadening due to the coupling with the spin system respectively. Here γ is the spin decay rate, *g* is the *g*-factor (or the effective g-factor) and $x = \mu_B B_0/h$. The collective coupling strength is [Fernando]:

$$\Omega = g_{eff} \frac{\mu_B}{h} \sqrt{n \int_V \left| \langle G | \, \vec{b}_{rms} \cdot \vec{S} | E \rangle \right|^2 dV} \qquad (2)$$

where $|\mathrm{E}\rangle$ and $|\mathrm{G}\rangle$ are the excited and ground state coupled by the dipolar magnetic transitions, $\vec{\mathrm{b}}_{\mathrm{rms}}$ is the vacuum magnetic field of the cavity, n is the (uniform) density of spins and $g_{eff}^2 = \mathrm{g}_{\mathrm{eff},||}^2 \cos^2\vartheta + \mathrm{g}_{\mathrm{eff},\perp}^2 \sin^2\vartheta$, where ϑ is the angle formed by the magnetic anisotropy axis of the molecule with the applied magnetic field. The previous expression can be simplified by introducing the single-spin coupling strength Ω_s, which takes into account the matrix element of the spin transition and the intensity of the magnetic component of the vacuum cavity field [spin_impurities]. In this way, the collective coupling strength simply results:

$$\Omega = \Omega_s \sqrt{N_{eff}} \qquad (3)$$

where $N_{eff} = n\,V$ is the number of polarized spins and V is the volume of the sample. The spin density *n* depends on temperature according to the Brillouin function, which for spin ½ paramagnets reads [APL]:

$$n = n_0 \, tanh\left(\frac{h\nu_0}{2k_B T}\right) \qquad (4)$$

where n_0 is the room temperature spin concentration of the crystal. It turns out from Eq. (3) and (4) that the effective coupling depends on the concentration of magnetic centers and their polarization at different temperatures.

Data analysis. We now focus our data analysis on the main lines of respective spectra and we concentrate on the coupling parameters Ω (and Ω_s for a single spin) and on the linewidth γ, which are extracted by fitting curves with Eqs. (1) and that are summarised in Table 1. Notice that the additional hyperfine transitions have lower intensities with respect to the main EPR resonance and the coupling rates are typically smaller while the line widths are comparable -or even larger- with respect to the main lines. Here we just point out that the decay rate of our resonator is k_0≈ 0.3 MHz [ESI] and always fulfils the condition $\Omega > k_0$. In addition, the mean cavity photon number spans from ≈10^{11} (P_{in}=-13 dBm) down to ≈10^5 (P_{in}=-73 dBm) thus the weak excitation limit $N_{eff} >> n$ is always satisfied in our experiments.

In comparison with the lanthanide complexes investigated here, the magnetic transitions in diluted (2%) and deuterated $Cu(mnt)_2$ single crystal show a sharper linewidth, which is about 6 MHz at 2 K for the main line (Table 1). For this particular resonance the collective coupling strength is Ω=2.73 MHz. Taking into account the estimated number of polarized spins N_{eff} ≈ 7.4 x 10^{14}, the single-spin coupling strength is Ω_s=0.1 Hz. This value is lower than what obtained for DPPH

Sample	*g*-factor	γ (MHz)	N_{eff} (T=2 K)	Ω (MHz)	Ω_s (Hz)
$Cu(mnt)_2$ 2%	2.04 ± 0.01	6.2 ± 0.5	$7.4 \cdot 10^{14}$	2.7 ± 0.5	0.10 ± 0.05
$[ErPc_2]^-TBA^+$ 10%	9.21 ± 0.01	410 ± 10	$6.5 \cdot 10^{14}$	27.1 ± 3.0	1.0 ± 0.2
Dy-trensal 3%	9.93 ± 0.02	471 ± 38	$8 \cdot 10^{13}$	16.2 ± 2.0	1.8 ± 0.3

Table 1: Summary of the parameters extracted by fitting the experimental data with Eq. 1a and 1b. The values reported in the table correspond to the most intense observed line of each molecule. For each compound, the reported line also corresponds to the ones with the lowest value of line width (θ=90°).

organic radicals (0.6 Hz) with the same YBCO resonator [APL]. We attribute this difference to the hyperfine splitting in $Cu(mnt)_2$, which results in the molecules being distributed over four hyperfine levels, thus decreasing the effective number of molecules in the ensemble.

The comparison between the parameters of $Cu(mnt)_2$ and those of $[ErPc_2]^-TBA^+$ and Dy-trensal shows larger values of the collective coupling strength for the latter (Table 1). For $[ErPc_2]^-TBA^+$ (θ=90°), we extracted Ω=27.1 MHz from the fit of the experimental data (Figure 6). Given the estimated number of polarized spins $N_{eff}=6.5\cdot10^{14}$, from Eq. 3 we obtain Ω_s=1 Hz. A similar result was obtained for Dy-trensal (θ=90°). The fit of the experimental curves shown in Figure 7 gives $\Omega\approx16.2$ MHz, which, in turns, leads to Ω_s=1.8 Hz by considering $N_{eff}=8\cdot10^{13}$ spins. On the other hand, the fitted linewidths result 410 MHz and 471 MHz for $[ErPc_2]^-TBA^+$ and Dy-trensal respectively. These values are far larger than those obtained for $Cu(mnt)_2$. Molecules with single lanthanides show superior coupling strengths but, since the linewidth of the principal spin transition are broader than for $Cu(mnt)_2$, the ratio Ω/γ results to be smaller for $[ErPc_2]^-TBA^+$ and Dy-trensal. Experiments with Lanthanides samples with lower spin concentrations did not show a significant reduction of the measured linewidth γ. This suggests that the main limitation is probably due to the inhomogenous broadening in our experiments (see Figure 7 of theESI).

We can conclude that for the $Cu(mnt)_2$ 2% diluted and deuterated crystal the collective coupling strength Ω results to be approximately 2.3 times smaller than the linewidth γ, thus below the strong coupling regime although not much far from it. The $[ErPc_2]^-TBA^+$ and Dy-trensal samples used in our experiments are still further away from the strong coupling regime with our YBCO resonator, in spite of the their enhanced single-spin coupling strength. Notice that the transitions reported in Table 1 for the lanthanide single-ion molecules are obtained by applying the magnetic field about the easy plane of magnetization, as indicated by the large *g*-factor. The magnetic component of the microwave field, which oscillates perpendicular to the YBCO central strip, is thus applied about the hard direction. According to Ref. [Er_doped], higher coupling strengths should be obtained in the orthogonal direction (external magnetic field in the hard direction and microwave field in the easy plane). However, our results reported in Figure S4,S6 and Table S1,S2 of the ESI show for these transitions weak intensity and broad lines.

Figure 8 summarizes the main results obtained in our experiments in term of coupling rate Ω and spin linewidth γ. The $\Omega=\gamma$ dashed line is depicted to show the threshold between the weak and strong coupling regimes. Since $\gamma, \Omega > \kappa_0$, these can be simply visualized below and above the $\Omega > \gamma$ dashed line, respectively. We also add the results for DPPH and PyBTM radical reported in [APL] and [PyBTM] respectively, in which the strong coupling condition was fulfilled with our set up. Further results reported in literature for similar spectroscopic experiments with Nitrogen Vacancy centers [spin_impurities] and Er ions in Y_2SiO_5 [Bushev,Er_doped] coupled to Niobium coplanar resonators at 10-50 mK are also shown for comparison. Figure 8 shows that the best conditions in terms of coherent coupling are obtained for $Cu(mnt)_2$ 2% diluted and deuterated crystal in our experimental conditions. The effect of lowering concentration certainly helps in getting sharper lines, yet the collective coupling is also scaled down with number of spin centers and the total benefit seems to be washed out for certain values of dilution.

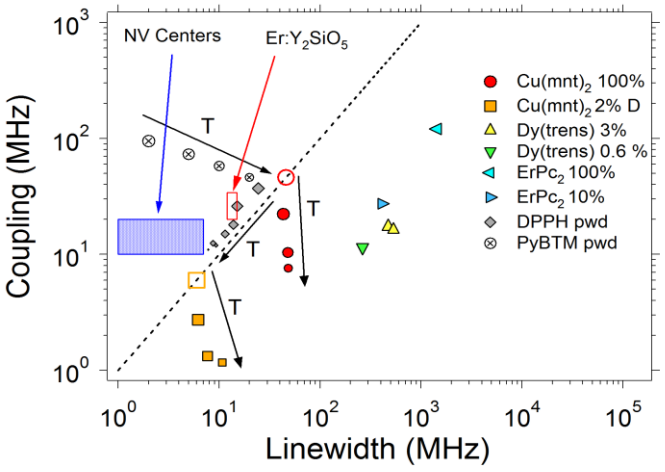

Figure 8: Plot of coupling rate and spin linewidth parameters obtained by fitting the experimental data with Eqs. 1 (filled symbols). Black arrows with T and the size of symbols represent the temperature evolution, from 2K (larger symbols) to 50 K (small symbols). Open circles display the parameters extrapolated to 0.3 K by means of Eq. 4. The dashed line indicates $\Omega = \gamma$. The parameters of DPPH and PyBTM organic radicals (measured between 2 and 70K) are taken form [APL] and [PyBTM] respectively. The rectangles show the typical values obtained for NV centers [spin_impurities] and $Er:Y_2SiO_5$ [Er_doped] at 10-50 mK.

As an example, for the 2% $Cu(mnt)_2$ (which has the advantages given by the deuteration [Bader]), concentrations values of 10^{15}-10^{16} spin/cm^3 are needed to get γ below 10 MHz.

However, such low concentrations make the collective coupling and the signal too low in our experiments.

Alternatively, we can consider the effect of the temperature. For this, we also plot the Ω vs γ parameters estimated between 2 and 70 K at which experiments were systematically repeated. It turns out that lowering the temperature increases the collective coupling Ω since the number of spins aligned with the magnetic field increases and, at the same time, the linewidth gets –slightly- sharper. Both effects may eventually lead to the strong coupling regimes. By simply extrapolating the curves in Figure 8 we can estimate that working at 0.3 K could allow to reach the strong coupling for $Cu(mnt)_2$ 2% diluted and deuterated crystal. Notice that this temperature is about 10 times higher with respect to the temperatures used for NV-centers and $Er:Y_2SiO_5$ ions thus showing that molecular spin centers can actually be competitive with respects to spin defects in inorganic solids.

Conclusions

In conclusion we have investigated different molecular magnetic centers at low temperatures by means of superconducting YBCO resonators looking for strong coupling regime. The collective coupling Ω and the spin linewidth γ were systematically investigated for different dilutions and orientations of magnetic centers. Lanthanides-based molecules were found to have high coupling strength but also the broadest spin linewidths. Mononuclear molecular $Cu(mnt)_2$ can have linewidths comparable with typical values reported for NV centers and $Er:Y_2SiO_5$ ions. In particular, the 2% deuterated $Cu(mnt)_2$ was found to have the minimum linewidth of 6 MHz. Despite this, the coupling strength at 2 K is not sufficient to achieve the strong coupling regime, although not much far from it.

The origin of the main limitation in reducing the essential parameter γ of our experiments still needs to be clarified: on one hand, the single molecule relaxation and coherence times T_1 and T_2 both contribute to the collective linewidth γ, on the other hand inhomogeneous broadening is also playing a role on the final results. In the case of $[ErPc_2]^-TBA^+$ part of the line broadening comes from the convolutions of two resonances related to the two orientations of molecules in the crystalline structure. Furthermore, isotopic enrichment performed on the even Rare Earth isotopes (I=0) could help in the reduction of hyperfine contributions to the main lines. These issues need to be controlled in a better way in order to design new molecular crystals suitable for circuit-QED experiments.

Acknowledgements

We wish to thank S. Klyatskaya (Karlsruhe Institute of Technology) for additional $ErPc_2^-[TBA]^+$ sample preparation and characterization. This work was partially funded by the Italian Ministry of Education and Research (MIUR) through "Fondo Investimenti per la Ricerca di Base" (FIRB) Project RBFR12RPD1, by the U.S. AFOSR/AOARD program, Contract No. FA2386-13-1-4029 and by the European FP7 FET project MoQuaS contract N.610449.

References

1 [GTA] A. Ghirri, F. Troiani, and M. Affronte, in Molecular Nanomagnets and Related Phenomena - Structure and Bonding (Edited by: S. Gao, Springer, Berlin, 2015).

2 [DEC] P. C. E. Stamp, A. Gaita-Ariño, *J. Mater. Chem.,* 2009*, 19*, 1718-1730.

3 [Nori] Z.-L. Xiang, S. Ashhab, J. Q. You, and F. Nori, *Rev. Mod. Phys.*, 2013, **85**, 623.

4 [APL] A. Ghirri, C. Bonizzoni, D. Gerace, S. Sanna, A. Cassinese and M. Affronte, *Appl. Phys. Lett.*, 2015, **106**, 184101.

5 [Bienfait] A. Bienfait, J. J. Pla, Y. Kubo, M. Stern, X. Zhou, C. C. Lo, C. D. Weis, T. Schenkel, M. L. W. Thewalt, D. Vion, D. Esteve, B. Julsgaard, K. Mølmer, J. J. L. Morton and P. Bertet, *Nat. Nanotech.*, 2016, **11**, 253.

6 [TavisCummings] I. Chiorescu, N. Groll, S. Bertaina, T. Mori, and S. Myiashita, *Phys. Rev. B*, 2010, **82**, 024413; Z. Kurucz, J. H. Wesenberg and K. Molmer, *Phys. Rev. A*, 2011, **83**, 053852; I. Diniz, S. Portolan, R. Ferreira, J. M. Gerard, P. Bertet and A. Auffeves, *Phys. Rev. A*, 2011, **84**, 063810.

7 [spin_impurities] Y. Kubo, F. R. Ong, P. Bertet, D. Vion, V. Jacques, D. Zheng, A. Dreau, J. F. Roch, A. Auffeves, F. Jelezko, J. Wrachtrup, M. F. Barthe, P. Bergonzo, and D. Esteve, *Phys. Rev. Lett.*, 2010, **105**, 140502; D. I. Schuster, A. P. Sears, E. Ginossar, L. DiCarlo, L. Frunzio, J. J. L. Morton, H. Wu, G. A. D. Briggs, B. B. Buckley, D. D. Awschalom, and R. J. Schoelkopf, *Phys. Rev. Lett*., 2010, **105**, 140501; R. Amsuss, C. Koller, T. Nobauer, S. Putz, S. Rotter, K. Sandner, S. Schneider, M. Schrambock, G. Steinhauser, H. Ritsch, J. Schmiedmayer, and J. Majer, *Phys. Rev. Lett*., 2011, **107**, 060502.

8 [Er_doped] S. Probst, H. Rotzinger, S. Wunsch, P. Jung, M. Jerger, M. Siegel, A.V. Ustinov and P. A. Bushev, *Phys. Rev. Lett*., 2013, **110**, 157001; A. Tkalcec, S. Probst, D. Rieger, H. Rotzinger, S. Wunsch, N. Kukharchyk, A. D. Wieck, M. Siegel, A. V. Ustinov, and P. Bushev, *Phys. Rev. B*, 2014, **90**, 075112.

9 [PyBTM] A. Ghirri, C. Bonizzoni, F. Troiani, N. Buccheri, L. Beverina, A. Cassinese and M. Affronte, arXiv:1605.02879 [cond-mat.mes-hall]

10 [Abe] E. Abe, H. Wu, A. Ardavan and J. J. L. Morton, *Appl. Phys. Lett.*, 2011, **98**, 251108.

11 [long_Tm] M. Warner, S. Din, I. S. Tupitsyn, G. W. Morley, A. M. Stoneham, J. A. Gardener, Z. Wu, A. J. Fisher, S. Heutz, C. W. M. Kay and G. Aeppli, *Nature*, 2013, **503**, 504; J. M. Zadrozny, J. Niklas, O. G. Poluektov, and D. E. Freedman, *ACS Cent. Sci.* 2015, **1**, 488; M. Atzori, L. Tesi, E. Morra, M. Chiesa, L. Sorace and R. Sessoli*, J. Am. Chem. Soc*., 2016, **138**, 2154.

12 [Bader] K. Bader, D. Dengler, S. Lenz, B. Endeward, S.-D. Jiang, P. Neugebauer and J. van Slageren, *Nat. Commun*. 2014, **5**, 5304.

13 [Stach] J. Stach, R. Kirmse, W. Dietzsch and E. Hoyer, *Inorg. Nucl. Chem. Letters*, 1978, 14, 143.

14 [Fernando] M. Jenkins, T. Hümmer, M. J. Martínez-Pérez, J. García-Ripoll, D. Zueco and F. Luis, *New Journal of Physics*, 2013, 15.

15 [Lewis] G. R. Lewis and I. Dance, *J. Chem. Soc., Dalton Trans.,* 2000*,* 3176.

16 [Ishikawa03] N. Ishikawa, M. Sugita, T. Okubo, N. Tanaka, T. Iino and Y. Kaizu, *Inorg. Chem*., 2003, **42**, 2440.

17 [Flanagan] B. M. Flanagan, P. V. Bernhardt, E. R. Krausz, S. R. Luthi and M. J. Riley*, Inorg. Chem*. 2002, **41**, 5024.

18 [Pedersen] K. S. Pedersen, L. Ungur, M. Sigrist, A. Sundt, M. Schau-Magnussen, V. Vieru, H, Mutka, S. Rols, H. Weihe, O.

Waldmann, L. F. Chibotaru, J. Bendix and J. Dreiser, *Chem. Sci.*, 2014, **5**, 1650.
19 [Lucaccini] E. Lucaccini, L. Sorace, M. Perfetti, J.-P. Costes and R. Sessoli, *Chem. Commun.*, 2014, **50**, 1648.
20 [Perfetti] M. Perfetti, E. Lucaccini, L. Sorace, J. P. Costes and R. Sessoli, *Inorg. Chem.*, 2015, **54**, 3090.
21 [Marx] R. Marx, F. Moro, M. Dorfel, L. Ungur, M. Waters, S. D. Jiang, M. Orlita, J. Taylor, W. Frey, L. F. Chibotaru and J. van Slageren, *Chem. Sci.*, 2014, **5**, 3287.
22 [AbragamBleaney] A. Abragam and B. Bleaney, *Electron Paramagnetic Resonance of Transition Ions*, Dover, New York, 1986.
23 [Bushev] P. Bushev, A. K. Feofanov, H. Rotzinger, I. Protopopov, J. H. Cole, C. M. Wilson, G. Fischer, A. Lukashenko, and A. V. Ustinov, *Phys. Rev. B*, 2011, **84**, 060501(R).

